

Research Article

Jicheng Jin, Jian Lu and Bo Zhen*

Resonance-forbidden second-harmonic generation in nonlinear photonic crystals

<https://doi.org/10.1515/nanoph-2021-0379>

Received July 14, 2021; accepted September 21, 2021;
published online October 5, 2021

Abstract: Second harmonic generation through nonlinear nano-photonic structures is important in both classical and quantum applications. It is commonly expected that the second harmonic frequency can always be generated as long as appropriate quadratic nonlinearity is provided by the material and the phase-matching condition is satisfied. Here, we present an anomaly to this common wisdom by showing that second-harmonic dipoles generated in a nonlinear photonic crystal slab can be completely nonradiative. As a result, no energy is transferred from the fundamental frequency to the second harmonic even when the phase-matching condition is satisfied – a phenomenon we call “resonance-forbidden second-harmonic generation”. Through numerical simulation, we identify two mechanisms that can achieve this phenomenon: symmetry protection and parameter tuning. The finite-size effect and the topological origin of this phenomenon are also discussed.

Keywords: nonradiating photonics; photonic crystal slabs; second-harmonic generation.

1 Introduction

Manipulation of light using nano-structures has always been of interest. One type of widely studied structures is the photonic crystal (PhC) slabs [1]. PhC slabs are dielectric slabs with periodically modulated refractive indices. The periodic modulation gives rise to photonic bands,

which are analogous to electric bands in solids. In general, PhC modes in the radiation continuum are resonances with finitely-long lifetime, as they can radiate to the far field. Such resonances are of importance in many applications, including photonic crystal surface emitting lasers [2], phase modulators [3, 4], and bio-sensors [5]. Interestingly, an unusual type of resonances, called bound states in the continuum (BICs), have been discovered in PhC slabs [6–8] and raised great interests over the past decade. Different from ordinary resonances, while BICs reside in the radiation continuum, they do not couple to the far-field radiation and thus maintain infinitely-long lifetime in theory. Various mechanisms to construct BICs have been identified and demonstrated in PhC slabs, including symmetry protection [6], parametric tuning [7, 9], and optical anisotropy [10]. The topological nature of BICs was also discovered to be vortex centers of polarization in PhC slabs [11]. So far, most applications of BICs are based on their properties in the linear regime, including high quality factor (Q) guided resonances robust to scattering [12] and unidirectional grating couplers [13]. Here, we extend the concept of BICs into the nonlinear optical regime. Specifically, we show that it is possible to construct patterns of nonlinear dipoles, which live in the radiation continuum but do not radiate – a phenomenon we name as “resonance-forbidden second-harmonic generation (SHG)”.

Recent developments in the growth and fabrication of nonlinear optical materials greatly benefit the research in nonlinear nano-photonics. Nonlinear materials including AlN [14], GaAs [15], GaSe [16], and LiNbO₃ [17, 18] can be now made into slabs with high index contrasts via techniques such as direct growth [14], suspension [19], exfoliation [16], and wafer-bonding [15]. This capability has enabled various applications, such as resonance-enhanced harmonic generation [20–24] and integrated quantum optics [19], where optical resonances are often utilized to enhance optical nonlinearity. Our presented idea of “resonance-forbidden SHG” is the opposite: we show that SHG through certain resonances can be completely forbidden. Specifically, while both the fundamental resonance and its second harmonic field are in the radiation continuum, the nonlinear dipole cannot radiate into

*Corresponding author: Bo Zhen, Department of Physics and Astronomy, University of Pennsylvania, Philadelphia, Pennsylvania, 19104, USA, E-mail: bozhen@sas.upenn.edu. <https://orcid.org/0000-0001-8815-3893>

Jicheng Jin and Jian Lu, Department of Physics and Astronomy, University of Pennsylvania, Philadelphia, PA, 19104, USA, E-mail: jichengj@sas.upenn.edu (J. Jin), jianlu@sas.upenn.edu (J. Lu)

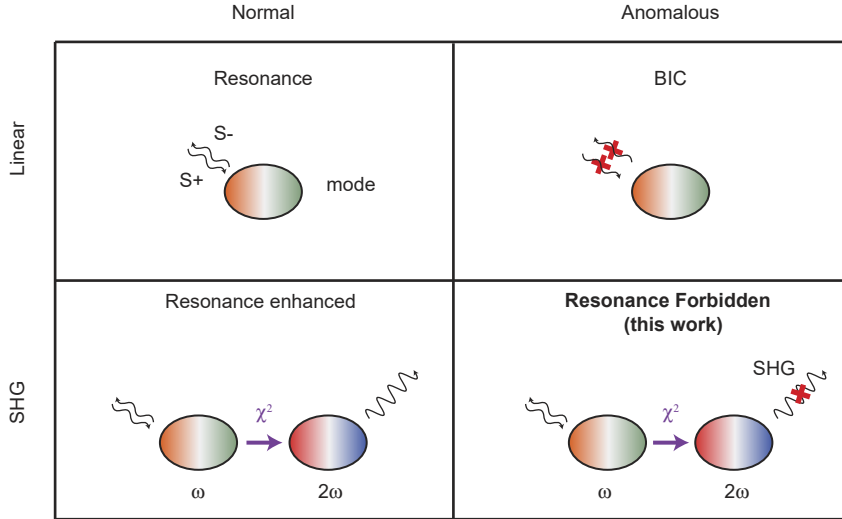


Figure 1: Basic concept of this work. Top row: unlike normal resonances, bound states in the continuum (BICs) in linear optical systems do not couple to the radiation channels. Bottom row: in this work, we show that instead enhancing the SHG like in most resonances, SHG can be completely forbidden in certain cases, which we name “resonance-forbidden SHG”.

the free space. As a result, no pump energy is converted into the second harmonic frequency. We note that, unlike phase-mismatching that is often used to suppress SHG in the lateral direction, our method focuses on suppressing SHG in the vertical direction.

To clarify the basic concept of “resonance-forbidden SHG”, we draw an analogy to BICs as shown in Figure 1. In linear optical systems, most resonances radiate into and, thus, can be excited from the far-field through channel S_- and S_+ , respectively. As an anomaly to this common wisdom, BICs cannot couple to radiation and their quality factors Q diverge into infinity. Similar phenomena of non-radiating photonics can also happen in nonlinear optical systems. When a nonlinear resonance at frequency ω is excited, nonlinear dipoles at 2ω are generated through quadratic susceptibilities $\chi^{(2)}$, which often can radiate into the far field – a process often known as “resonance-enhanced SHG” [22, 25, 26]. Interestingly, we show that

anomalous behaviors can also happen in this SHG process, where generated nonlinear dipoles cannot radiate into the far field though living inside the radiation continuum. As a result, SHG is completely suppressed and no pump energy is converted into the second harmonic frequency, even when the phase-matching condition is satisfied. Here, we note that different from BICs, which are resonances of the structure, the generated nonlinear dipoles do not correspond to eigenmodes of the underlying structure.

2 Results

2.1 Resonance-forbidden SHG by symmetry

We start by showing how SHG can be forbidden by the symmetry-mismatch between the SH dipoles and free-space modes. As shown in Figure 2a, a 1D PhC slab is

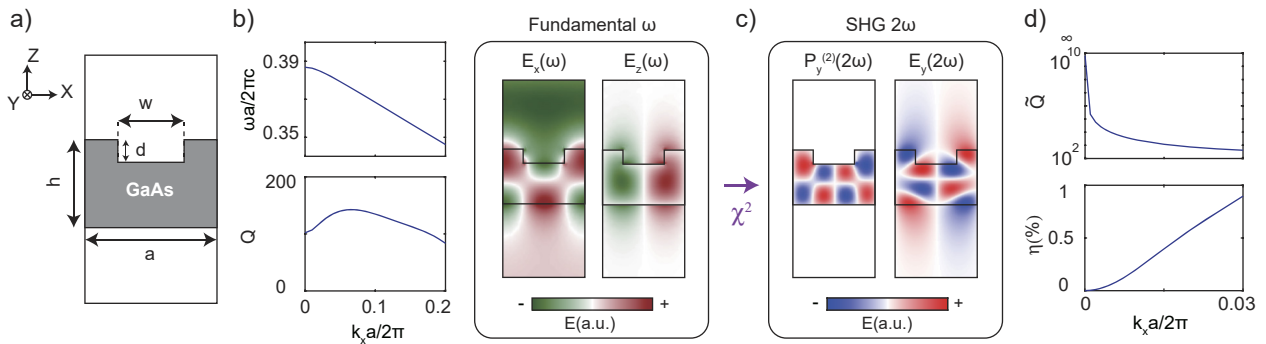


Figure 2: Symmetry-forbidden SHG through nonlinear resonances. (a) Schematic drawing of a 1D GaAs PhC slab unit cell. (b) The band structure and quality factor (Q) of a TE band. Mode profiles of E_x and E_z components at the Γ point are both odd under the C_2^z operation. (c) Through the quadratic nonlinearity of GaAs, the resonance at Γ induces nonlinear polarization $\mathbf{P}_y^{(2)}$ and electric field $\mathbf{E}_y^{(2)}$ at frequency (2ω), both of which are even under C_2^z . (d) Due to symmetry mismatch, the induced SH dipoles cannot radiate, leading to a divergence of \bar{Q} at Γ , which is inversely proportional to SHG efficiency η . $a = 600$ nm. $h = 400$ nm. $w = 300$ nm. $d = 100$ nm. The pump field is set to be 1 GV/m.

uniform along y and periodic along x . Air gaps of width $w = 300$ nm and depth $d = 100$ nm are etched into the GaAs slab of thickness $h = 400$ nm at a periodicity of $a = 600$ nm. In the linear regime, resonances in such a structure can be well-understood using symmetry. Specifically, this structure is invariant under the 180° rotation around the z -axis, C_2^z , which changes \hat{x} to $-\hat{x}$ and \hat{y} to $-\hat{y}$. At the center of the momentum space, Γ , modes that are even under C_2^z are BICs with diverging Q .

Instead, here we focus on a transverse-electric (TE) mode that is odd under C_2^z with a finite Q of about 100. Specifically, this TE mode has field components of H_y , E_x , and E_z . The eigenfrequencies ω and quality factors Q of the second lowest TE band is shown in Figure 1b, together with its mode profile at Γ . As shown, the mode profile is indeed odd under C_2^z . We now compute the SHG efficiency through this resonance via the quadratic nonlinear susceptibilities of GaAs, of which the non-zero terms are $\chi_{xyz}^{(2)}$ and its permutations. Accordingly, this TE mode of interest can only create SH dipoles along y :

$$\mathbf{P}_y^{(2)} = 2\epsilon_0\chi_{yzx}^{(2)}\mathbf{E}_x\mathbf{E}_z = 4\epsilon_0d_{25}\mathbf{E}_x\mathbf{E}_z. \quad (1)$$

Here, $d_{25} = 119$ pm/V is the quadratic nonlinearity of GaAs. A simple calculation reveals that the nonlinear dipole $\mathbf{P}^{(2)}$ is even under C_2^z :

$$\hat{O}_{C_2^z}\mathbf{P}^{(2)}(\mathbf{r}) = C_2^z\mathbf{P}^{(2)}(C_2^z\mathbf{r}) = \mathbf{P}^{(2)}(\mathbf{r}). \quad (2)$$

This symmetry analysis is confirmed by the distribution of the SH dipoles $\mathbf{P}_y^{(2)}$ and the SH field $\mathbf{E}_y^{(2)}$ as shown in Figure 2c. By satisfying the sub-wavelength condition, the SH field is below the diffraction limit, allowing only one radiation channel available to the SH dipoles. Meanwhile, due to symmetry-mismatch, the SH dipoles cannot radiate into free-space; accordingly, no energy is transferred to the SH frequency and the SHG efficiency remains 0, despite the existence of optical nonlinearity. Again, we emphasize that neither the fundamental resonance nor the second harmonic dipoles correspond to a BIC: the fundamental resonance has a finite Q of about 100. Meanwhile, the second harmonic dipoles do not correspond to a resonance of the underlying structure.

To quantitatively evaluate the radiation efficiency of SH dipoles, we define parameter \tilde{Q} of a nonlinear resonance in a similar way as the quality factor Q of a linear resonance:

$$\tilde{Q} = 2\pi f \frac{E}{P}. \quad (3)$$

Here, E is the energy stored in SH dipoles inside the slab. P is the radiation power of the SH field in the far field. f is the SH frequency, which is doubled from the fundamental frequency. We note that the nonlinear \tilde{Q} -factor is

different from the standard Q -factors of resonances, in that the nonlinear dipoles do not correspond to resonances or eigenmodes of the underlying structure. Naturally, \tilde{Q} diverges when “resonance-forbidden SHG” occurs, which is observed at the Γ point as shown in Figure 2d. The energy conversion efficiency $\eta = 1 - (T + R)$ is calculated by first computing how much of the pump energy is transmitted (T) or reflected (R). It can be seen that no pump energy is converted into the second harmonic frequency at the $k = 0$. When the momentum deviates from $k_x = 0$, the C_2^z symmetry is broken and \tilde{Q} becomes finite. In these cases, the SH dipoles can radiate to the far field, and the system returns to the “resonance-enhanced SHG” scenario instead.

2.2 Resonance-forbidden SHG through parameter-tuning

In this section, we present another example of “resonance-forbidden SHG” that cannot be explained by symmetry; instead, it relies on a different mechanism of parameter-tuning. The nonlinear PhC slab is schematically shown in Figure 3a. Air gaps of width $w = 30$ nm are etched all the way through a GaSe membrane with thickness of $h = 325.3$ nm at a periodicity of $a = 600$ nm. The band structure and Q of transverse-magnetic (TM) modes are plotted in Figure 3b, which only have out-of-plane electric field components \mathbf{E}_y .

The band of interest is highlighted in blue. The dispersion of the its SH field (red) is calculated by doubling the frequency and crystal momentum of the fundamental mode: $\omega_{\text{SHG}} = 2\omega_0$ and $k_{\text{SHG}} = 2k_0$. As shown, in the range of our interest, the SH field stays above the light line, but below the folded light line; accordingly, only one radiation channel is allowed for the SH field, which is beneficial in designing resonance-forbidden SHG. We further note that the SH fields (red curve) do not correspond to a resonance of the underlying structure.

In GaSe, the non-zero quadratic nonlinearity susceptibilities are $\chi_{yyy}^{(2)} = -\chi_{xxy}^{(2)} = -\chi_{yxx}^{(2)}$. Accordingly, only y -polarized SH dipoles can be created through TM modes:

$$\mathbf{P}_y^{(2)} = 2\epsilon_0\chi_{yyy}^{(2)}\mathbf{E}_y\mathbf{E}_y = 4\epsilon_0d_{21}\mathbf{E}_y\mathbf{E}_y. \quad (4)$$

Based on the distribution of $\mathbf{P}_y^{(2)}$, the SH fields $\mathbf{E}_y^{(2)}$ are computed for resonances at different k_x . See Methods for more details of the calculation.

Interestingly, “resonance-forbidden SHG” occurs at $k_x = 0.01 \times 2\pi/a$ in this structure, which is marked by a blue cross in Figure 3b. The SH dipole $\mathbf{P}_y^{(2)}$ and SH field $\mathbf{E}_y^{(2)}$ of the corresponding mode are shown in Figure 3c.

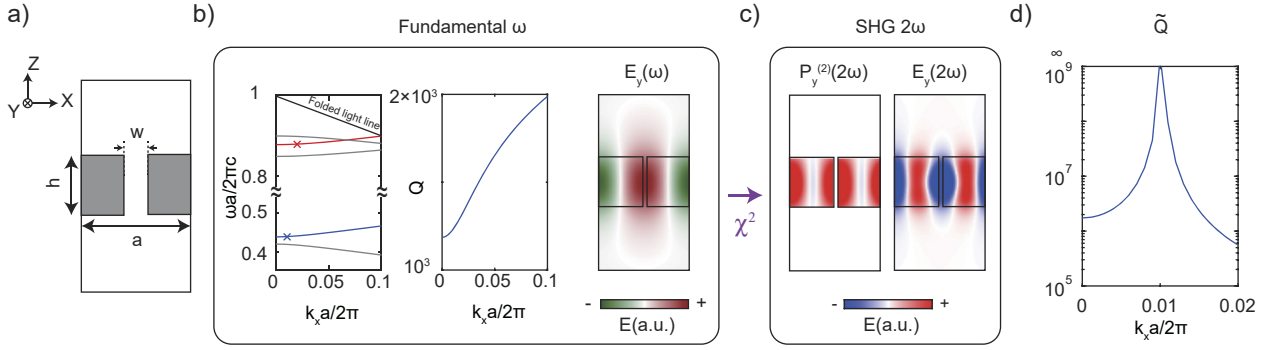


Figure 3: Forbidding SHG through parametric tuning. (a) Schematic drawing of a 1D GaSe PhC unit cell. (b) Calculated band structure and Q_s of the TM bands. One band of interest is shown in blue, along with the frequency and momentum of its second-harmonic fields shown in red. The mode of interest at $k_x = 0.01 \times 2\pi/a$ is marked by a cross. Its mode profile (E_y) is shown in colormap. (c) Distribution of the induced nonlinear polarization $P_y^{(2)}$ and second harmonic field E_y^2 . (d) \tilde{Q} diverges at $k_x = 0.01 \times 2\pi/a$, confirming that the resonance of interest forbids SHG. $a = 600$ nm. $h = 325.3$ nm. $w = 30$ nm.

As shown, the SH field only has an evanescent component in the free space with no far-field radiation. This is quantitatively confirmed in the \tilde{Q} plot, which diverges at $k_x = 0.01 \times 2\pi/a$ (Figure 3d). As the C_2^z symmetry is broken by the non-zero k_x , this “resonance-forbidden SHG” cannot be explained by symmetry alone and is based on a different mechanism of parameter-tuning.

2.3 Topological nature of resonance-forbidden SHG

In this section, we discuss the robustness of “resonance-forbidden SHG” and elucidate the fundamental nature of this phenomenon as topological defects in one dimension.

Following the Bloch’s theorem, the SH field generated by a resonance in the setup of Figure 3 can be written as $\mathbf{E}_y^{(2)}(k) = e^{i2kx} v_k(x)$ and v_k is a periodic function in x . Since the SH field is below the diffraction limit, there is only one

radiation channel with an amplitude of $c_0(k) = \langle v_k \rangle$. Here, $\langle \cdot \rangle$ denotes spatial averaging of the given function over a unit cell, which is the same as the zeroth-order Fourier coefficient of this given function.

For structures with up–down mirror symmetry, which is invariant under the operation of changing \hat{z} into $-\hat{z}$ (e.g. Figure 3), SH fields at the top and bottom surfaces are always related. c_0 for the structure in Figure 3 is plotted in Figure 4a. The sign of c_0 is flipped from positive to negative when k_x increases from 0 to $0.02 \times 2\pi/a$. Accordingly, the phenomenon of “resonance-forbidden SHG” at $k_x a/2\pi = 0.01$ is fundamentally a topological defect of parameter c_0 , defined in the one dimensional space of k_x . Naturally, it exists in a robust manner when structural parameters are continuously varied. For example, as shown in Figure 4b, as the thickness of the GaSe slab h is continuously varied between 320 and 326 nm, the phenomenon of “resonance-forbidden SHG” can always be observed along the k_x axis.

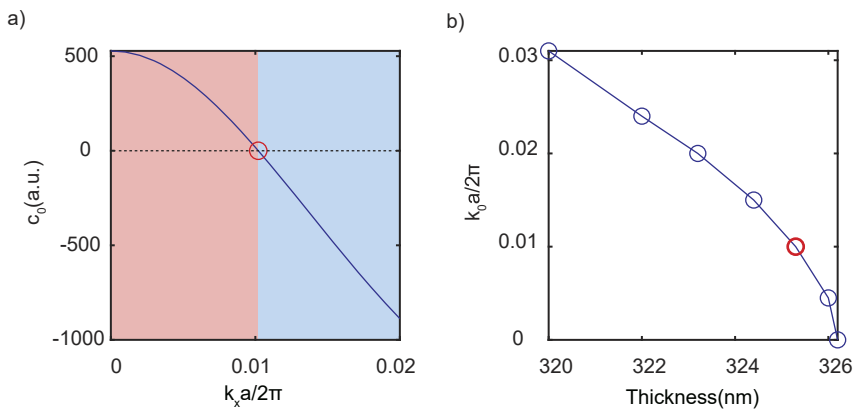


Figure 4: Robustness and topological origin of resonance-forbidden SHG. (a) For the structure shown in Figure 3, the radiation component of the SH field c_0 reduces to 0 at $k_x = 0.01 \times 2\pi/a$, where “resonance-forbidden SHG” occurs. This point, marked by a red circle, is fundamentally a topological defect between positive (red) and negative c_0 (blue). (b) “Resonance-forbidden SHG” can be robustly found at different k_x points when a structural parameter h is varied.

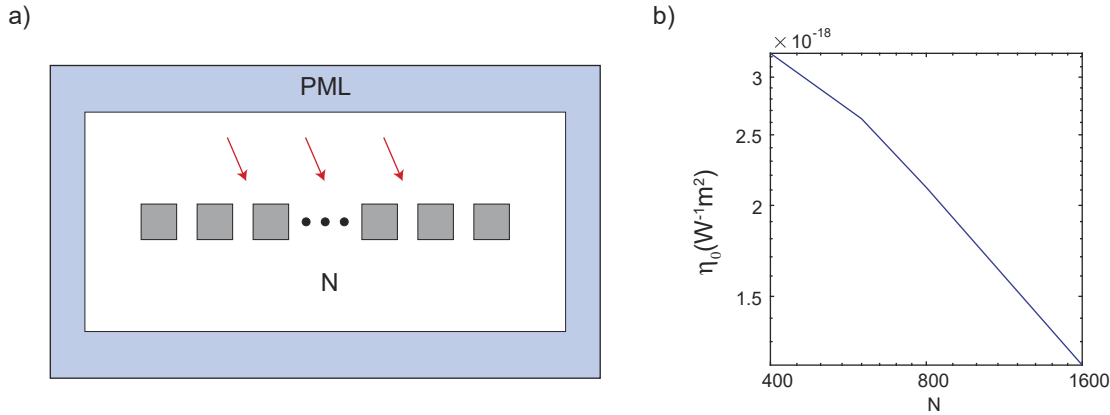


Figure 5: Finite-size effect on resonance-forbidden SHG. (a) A finite-size PhC slab of N unit cells with the same parameters as in Figure 3 is excited by a plane wave. Normalized SHG efficiency η_0 is simulated for different values of N . (b) The normalized SHG efficiency η_0 decreases as the sample size N increases.

2.4 Finite-size effect on resonance-forbidden SHG

In this section, we discuss the practical question of how SHG efficiency scales with the size of the nonlinear PhC slab. When the PhC slab is of a finite size, momentum k is no-longer perfectly conserved, and the generated nonlinear dipoles can always radiate into free space. To investigate how sample sizes affect the pump depletion rate, we simulate a finite-size PhC, consisting of N unit cells, which

is always pumped on-resonance with the mode of interest at $k_x a / 2\pi = 0.01$. The finite-size PhC in Figure 5a is surrounded by perfect matching layers (PMLs). The number of unit cells N is varied from 400 to 1600. Normalized conversion efficiency is calculated for each N , which is defined as $\eta_0 = I_{\text{SHG}} / (I_{\text{pump}})^2$. Here, I is the energy flux with a unit of W/m^2 . Our simulation results (Figure 5b) show that the normalized conversion efficiency η_0 decreases as the sample size increases. This can be intuitively understood: as the structure approaches infinitely large, the structure

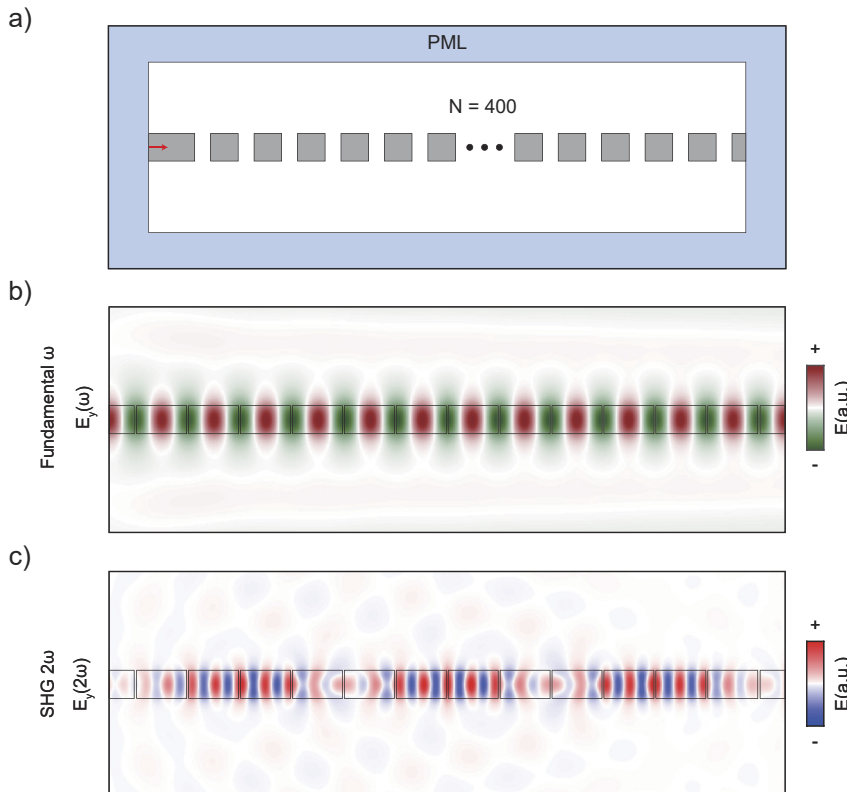


Figure 6: Effects of lateral excitation on resonance-forbidden SHG. (a) A PhC slab with the same design as in Figure 3 but of a finite length is excited through a wave-guide. The structure is surrounded with perfectly matched layers (PML). (b) The electric field distribution at the fundamental frequency ω within the first 13 unit cells is plotted. (c) The electric field generated at the SH-frequency 2ω shows an oscillation along the slab. The periodicity of the oscillation is defined by the in-plane momentum mismatch between the slab resonances at 2ω and the nonlinear dipoles.

recovers the periodic boundary condition as in Figure 3 and the normalized conversion efficiency is expected to reduce to 0. In experiment, we expect a large sample illuminated by a de-focused Gaussian beam to be a good enough approximation of an infinite structure and to observe this phenomenon of resonance-forbidden SHG.

2.5 Effects of lateral excitation through a waveguide

In this section, we discuss what happens when the resonance-forbidden SHG structure is excited on the side, such as through a waveguide. Different from the vertical excitation as before, the side coupling breaks the translation symmetry; as a result, the nonlinear dipoles will couple to eigenmodes of the underlying structure at the same frequency of 2ω , even if their in-plane momenta are quite different.

In simulation, a finite-size PhC slab consisting of $N = 400$ unit cells is excited through a waveguide (Figure 6a). The structural parameters of the PhC are the same with those in Figure 3. The excitation frequency ω is set to be on-resonance with the mode of interest at $k_x a / 2\pi = 0.01$. This fundamental mode propagates along the slab and decays exponentially due to its own radiation loss (Figure 6b). Meanwhile, the SH polarization generated by the fundamental mode can couple with all slab resonances at 2ω , as momentum is no longer conserved. As a result, the SH field oscillates along the x direction as shown in Figure 6c, which is similar to SHG in ordinary waveguides without a perfect phase-matching condition. Meanwhile, the coupling to slab resonances of finite quality factors also introduces vertical radiation loss, which is also observed in Figure 6c.

3 Conclusions

In summary, we extend the concept of nonradiating photonics into the nonlinear regime and introduce the phenomenon of “resonance-forbidden SHG”. We present two mechanisms to achieve this phenomenon, symmetry-mismatch and parameter-tuning, each illustrated through a numerical example. Finally, we elucidates the robustness of this phenomenon protected by its topological origin and the finite-size effect. Our method provides a new mechanism to manipulate SHG in nano-photonics structures, which could benefit nonlinear processes such as high harmonic generation by removing the pump depletion through SHG processes. Furthermore, our general method can also be applied to other general nonlinear processes beyond SHG, including third harmonic generation and

sum- and difference-frequency generation, to selectively forbid unwanted nonlinear processes.

4 Methods

The presented numerical examples are all computed using the finite element method in COMSOL 5.5. The band structures are calculated for a unit cell with periodic boundaries using an eigen-frequency solver. Based on these results, another simulation using the frequency domain solver is performed, which includes two sets of calculations, one for the fundamental frequency ω and the other for the SH frequency 2ω . For the calculation at ω , linear-polarized plane waves illuminate on the PhC under the on-resonance condition. For the calculation at 2ω , there is no incident wave. The two calculations are then coupled via nonlinear polarization using the “Multi-physics” function in COMSOL. The energy in the PhC slab and the radiation power of the SH field are extracted to compute \tilde{Q} . For calculations in the example of Figures 3–6, to preserve the up–down mirror symmetry of the structure, only the top half of the structure is included, which is terminated by a perfect magnetic conductor boundary. For all examples, the SH radiation coefficients, c_0 , are calculated using the SH field at the top surface of the slab.

Acknowledgment: J. J. and B. Z. conceived the idea. J. J. carried out numerical simulations. J. J., J. L. and B. Z. discussed and interpreted the results. J. J. and B. Z. wrote the paper with contribution from all authors. B. Z. supervised the project. We thank V. Yoshioka for helpful discussions.

Author contribution: All the authors have accepted responsibility for the entire content of this submitted manuscript and approved submission.

Research funding: This work was partly supported by the US Office of Naval Research (ONR) Multidisciplinary University Research Initiative (MURI) grant N00014-20-1-2325 and grant N00014-21-1-2703, and the Air Force Office of Scientific Research under award number FA9550-18-1-0133. J. L. was also supported by the Army Research Office under award contract W911NF-19-1-0087.

Conflict of interest statement: The authors declare no conflicts of interest regarding this article.

References

- [1] J. D. Joannopoulos, S. G. Johnson, J. N. Winn, and R. D. Meade, *Molding the Flow of Light*, Princeton, NJ [ua], Princeton Univ. Press, 2008.
- [2] K. Hirose, Y. Liang, Y. Kurosaka, A. Watanabe, T. Sugiyama, and S. Noda, “Watt-class high-power, high-beam-quality photonic-crystal lasers,” *Nat. Photonics*, vol. 8, no. 5, pp. 406–411, 2014.
- [3] H. Yu, A. Arbabi, and A. Faraon, “Reflective optical phase modulator based on high-contrast grating mirrors,” in *CLEO*:

- Science and Innovations*, Optical Society of America, 2014, p. STh4M.8.
- [4] J. Lv, X. Yin, J. Jin, et al., “Demonstration of a thermo-optic phase shifter by utilizing high-q resonance in high-index-contrast grating,” *Opt. Lett.*, vol. 43, no. 4, pp. 827, 2018.
- [5] M. El Beheiry, V. Liu, S. Fan, and O. Levi, “Sensitivity enhancement in photonic crystal slab biosensors,” *Opt. Express*, vol. 18, no. 22, pp. 22702–22714, 2010.
- [6] J. Lee, B. Zhen, S.-L. Chua, et al., “Observation and differentiation of unique high-q optical resonances near zero wave vector in macroscopic photonic crystal slabs,” *Phys. Rev. Lett.*, vol. 109, no. 6, p. 067401, 2012.
- [7] C. W. Hsu, B. Zhen, J. Lee, et al., “Observation of trapped light within the radiation continuum,” *Nature*, vol. 499, no. 7457, pp. 188–191, 2013.
- [8] C. W. Hsu, B. Zhen, A. D. Stone, J. D. Joannopoulos, and M. Soljačić, “Bound states in the continuum,” *Nat. Rev. Mater.*, vol. 1, p. 16048, 2016.
- [9] Y. Yang, C. Peng, Y. Liang, Z. Li, and S. Noda, “Analytical perspective for bound states in the continuum in photonic crystal slabs,” *Phys. Rev. Lett.*, vol. 113, no. 3, p. 037401, 2014.
- [10] J. Gomis-Bresco, D. Artigas, and L. Torner, “Anisotropy-induced photonic bound states in the continuum,” *Nat. Photonics*, vol. 11, no. 4, pp. 232–236, 2017.
- [11] B. Zhen, C. W. Hsu, L. Lu, A. S. Douglas, and M. Soljačić, “Topological nature of optical bound states in the continuum,” *Phys. Rev. Lett.*, vol. 113, no. 25, p. 257401, 2014.
- [12] J. Jin, X. Yin, L. Ni, M. Soljačić, B. Zhen, and C. Peng, “Topologically enabled ultrahigh-q guided resonances robust to out-of-plane scattering,” *Nature*, vol. 574, no. 7779, pp. 501–504, 2019.
- [13] X. Yin, J. Jin, M. Soljačić, C. Peng, and B. Zhen, “Observation of topologically enabled unidirectional guided resonances,” *Nature*, vol. 580, no. 7804, pp. 467–471, 2020.
- [14] L. Fan, C.-L. Zou, R. Cheng, et al., “Superconducting cavity electro-optics: a platform for coherent photon conversion between superconducting and photonic circuits,” *Sci. Adv.*, vol. 4, no. 8, p. eaar4994, 2018.
- [15] L. Chang, A. Boes, X. Guo, et al., “Heterogeneously integrated GaAs waveguides on insulator for efficient frequency conversion,” *Laser Photon. Rev.*, vol. 12, no. 10, pp. 1800149, 2018.
- [16] X.-T. Gan, C.-Y. Zhao, S.-Q. Hu, et al., “Microwatts continuous-wave pumped second harmonic generation in few- and monolayer gase,” *Light Sci. Appl.*, vol. 7, no. 1, pp. 17126, 2018.
- [17] M. Li, J. Ling, H. Yang, U. A. Javid, S. Xue, and Q. Lin, “Lithium niobate photonic-crystal electro-optic modulator,” *Nat. Commun.*, vol. 11, no. 1, p. 4123, 2020.
- [18] A. Boes, B. Corcoran, L. Chang, J. Bowers, and A. Mitchell, “Status and potential of lithium niobate on insulator (lnoi) for photonic integrated circuits,” *Laser Photon. Rev.*, vol. 12, p. 1700256, 2018.
- [19] S. Sun, H. Kim, Z. Luo, G. S. Solomon, and W. Edo, “A single-photon switch and transistor enabled by a solid-state quantum memory,” *Science*, vol. 361, no. 6397, pp. 57–60, 2018.
- [20] N. Bernhardt, K. Koshelev, S. J. U. White, et al., “Quasi-bic resonant enhancement of second-harmonic generation in ws2 monolayers,” *Nano Lett.*, vol. 20, no. 7, pp. 5309–5314, 2020.
- [21] R. Luo, H. Jiang, S. Rogers, H. Liang, H. Yang, and Q. Lin, “On-chip second-harmonic generation and broadband parametric down-conversion in a lithium niobate microresonator,” *Opt. Express*, vol. 25, no. 20, pp. 24531–24539, 2017.
- [22] J. Wang, M. Clementi, M. Minkov, et al., “Doubly resonant second-harmonic generation of a vortex beam from a bound state in the continuum,” *Optica*, vol. 7, no. 9, pp. 1126–1132, 2020.
- [23] Z. Liu, Y. Xu, Y. Lin, et al., “High-q quasibound states in the continuum for nonlinear metasurfaces,” *Phys. Rev. Lett.*, vol. 123, no. 25, p. 253901, 2019.
- [24] X. Zhang, Q.-T. Cao, Z. Wang, et al., “Symmetry-breaking-induced nonlinear optics at a microcavity surface,” *Nat. Photonics*, vol. 13, no. 1, pp. 21–24, 2019.
- [25] Z. Lin, X. Liang, M. Lončar, S. G. Johnson, and A. W. Rodriguez, “Cavity-enhanced second-harmonic generation via nonlinear-overlap optimization,” *Optica*, vol. 3, no. 3, p. 233, 2016.
- [26] M. Soljačić and J. D. Joannopoulos, “Enhancement of nonlinear effects using photonic crystals,” *Nat. Mater.*, vol. 3, no. 4, pp. 211–219, 2004.